**33RD CONGRESS
OF THE INTERNATIONAL COUNCIL
OF THE AERONAUTICAL SCIENCES
STOCKHOLM, SWEDEN, 4–9 SEPTEMBER, 2022**

**ICAS
2022
SWEDEN**

EFFECTS OF TWO WINGLET TIP GEOMETRIES ON THE FLOW AND AERODYNAMIC PERFORMANCE OF A HYDRAULIC AXIAL TURBINE

Daniel da Silva Tonon[1], Jesuino Takachi Tomita[1], Cleverson Bringhenti[1], Daniel Ferreira Corrêa Barbosa[1], Luiz Henrique Lindquist Whitacker[1] & Luiz Eduardo Nunes Almeida[2]

[1]Aeronautics Institute of Technology – ITA
[2]AVIBRAS

Abstract

An Axial Turbine Blade Tip has a great influence on its flow behavior and performance. Due to the clearance between the turbine casing and the rotor blades tips, part of the flow leaks from the pressure side to the suction side. This leakage reduces the turbomachine efficiency, and therefore must be minimized. Over the years, the use of desensitization techniques has proven to be an excellent strategy for reducing this unwanted flow. These techniques, however, has only been studied in machines that operate with compressible fluids. The objective of this work is to verify the effects of two Winglet geometries in the first stage of the Liquid Oxygen (LOX) Turbine used as booster in the Space Shuttle Main Engine (SSME). The two Winglet geometries evaluated have identical thickness and width, being differentiated by their trailing edge region configuration. In this region, the first geometry (*W1*) connects to the trailing edge with an angle close to 90°, while the second geometry (*W2*) presents a smooth connection. The results obtained show that it is possible to improve the stage efficiency depending on the geometry adopted, as well as to analyze the cavitation phenomenon. The mesh generation and simulations were done using a commercial software and the 3D flow calculations were based on the Reynolds Averaged Navier-Stokes (RANS) equations.

Keywords: Turbopump, CFD, Desensitization, Tip Clearance, Winglet.

Nomenclature

N	Rotational frequency, rpm.
$\dot{m}$	Passage mass flow, kg/s.
p	Averaged pressure, Pa.
η	Efficiency.
U	Tip circumferential velocity, m/s.
C	Velocity, m/s.
τ	Rotor total torque, N.m.
Z	Number of stator blades.
ρ	Density, kg/m^3.
R	Blade tip radius, m.

Subscripts

e	Outlet duct exit.
T	Total condition.
i	Inlet duct inlet.
0	Isentropic condition.

Acronyms

CFD	Computational Fluid Dynamics.

DP   Design Point.
ITA   Aeronautics Institute of Technology
LOX   Liquid Oxygen.
LPOTP   Low Pressure Oxidizer Turbopump.
NASA   National Aeronautics and Space Administration.
RANS   Reynolds Averaged Navier Stokes
RMS   Root Mean Square
SSME   Space Shuttle Main Engine.
SST   Shear Stress Transport

1. Introduction

Different studies have been developed over the years to analyze tip leakage effects on the axial turbomachines [1]. In addition to the fluid flow characteristics, the heat transfer at the blade tip region is also relevant and has been investigated in different works [2]-[4]. However, this work only presents analyzes regarding the aerodynamic characteristics of the flow in the tip region.

For constructive reasons, there must be a distance between the blade's tip and the turbine casing, since centrifugal forces, thermal expansion effects, and other operation turbomachines' characteristics cause geometric variations that could lead to catastrophic failures [5]. This tip clearance and the fact that there is a pressure difference between the blade sides allows the leakage of part of the working fluid through this region [6]. Naturally, the fluid that leaks does not participate in the transfer of energy to the turbine.

As already mentioned, the tip leakage has a great impact on the performance of the axial turbine and the flow field behavior. For these reasons, different works (whether numerical or experimental) were developed to quantify the losses generated by this leakage [7]-[12]. Also, many loss models have been developed to quantify the tip leakage effects during the axial turbomachines design [13]-[16].

Naturally, due to the negative effect generated by tip leakage, strategies to minimize this undesired flow started to be developed. These are called desensitization techniques and consist of geometric modifications on the blade's tip. These modifications are classified into squealer, winglet, and their combination called squealer-winglet. Figure 1 presents a comparison between these techniques with the flat tip geometry.
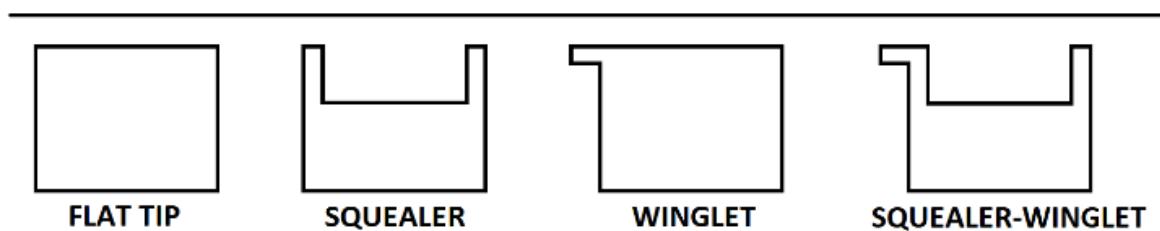
Figure 1 – Examples of blade tip geometries.

2. Objective

This work aims to analyze the aerodynamic effects of two winglet geometries in the first stage of the hydraulic axial turbine applied in the SSME LPOTP, to reduce the tip leakage and increase the performance of the analyzed stage. The results were obtained through simulations performed with CFX v. 19.2 software [17], distributed by ANSYS company. This work's results will be compared with those of previous research [18] and with the experimental results available in a NASA report [19]. Figures 2 and 3 show the representation of the SSME LPOTP and its turbine first stage, respectively.

The study performed in this work is the continuation of a series of other works developed in the Turbomachinery Department at ITA evaluating different desensitization techniques in the SSME LPOTP.
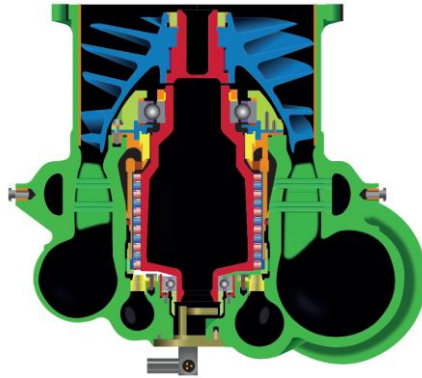
Figure 2 – LPOTP used in the SSME engine [20].

Figure 3 – 3D view of the LPOTP turbine first stage [21].

3. A brief review on the Winglet desensitization techniques

The winglet technique is one of the desensitization techniques used to prevent tip leakage. This is an aerodynamic component positioned on the blade tip, which projects out of the sides of the blade [1]. When this aerodynamic component projects out the pressure side, it is called the pressure side winglet; if it projects out the suction side, is called the suction side winglet; and if it projects out both blade sides, is called the total winglet. In this work, only pressure side winglets were studied. Figure 4 shows a representation of a pressure side winglet.
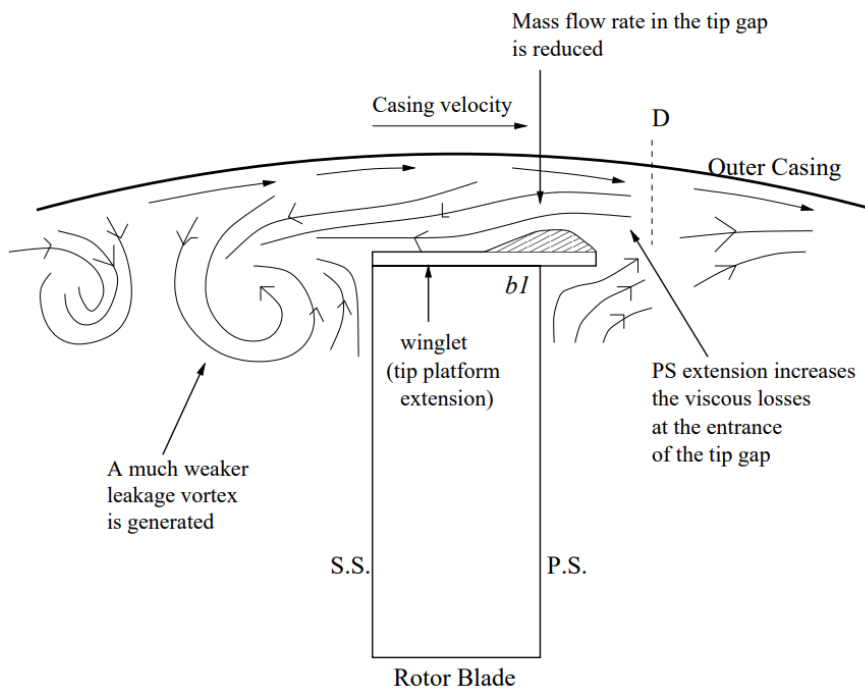
Figure 4 – Pressure side winglet geometry [22].

In the internal flow of the axial turbines, a leakage vortex is formed near the tip of the rotating blades. This vortex is responsible for a significant part of the viscous losses of these turbomachines. A geometric extension of the pressure side at the blade tip can significantly affect the flow behavior in this region, weakening the leakage vortex [1], as shown in Figure 4. There are many works in the open literature evaluating the application of the winglet techniques, among them [23]-[28].

Usually, this modification is parameterized according to its thickness and width, as shown in Figure 5.
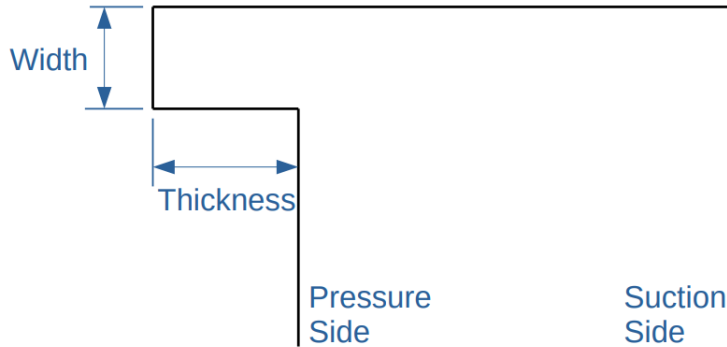
Figure 5 – Pressure side winglet dimensions.

4. Winglet geometries analyzed and mesh dependence study

The Winglet geometries analyzed in this work consider thickness and width values of 8.70% and 5.40%, respectively, both of these percentages in relation to the blade height. The difference between each of these geometries is in geometric modification connection at the rotor blade trailing edge. In the first geometry (*W1*), this connection is made with an angle close to 90°. For the second geometry (*W2*) the union between the Winglet and the blade is done smoothly. Figure 6 shows each of these geometries, illustrating the difference in the trailing edge region. The thickness and width values selected are part of a study of different Winglet geometries that will be published soon.
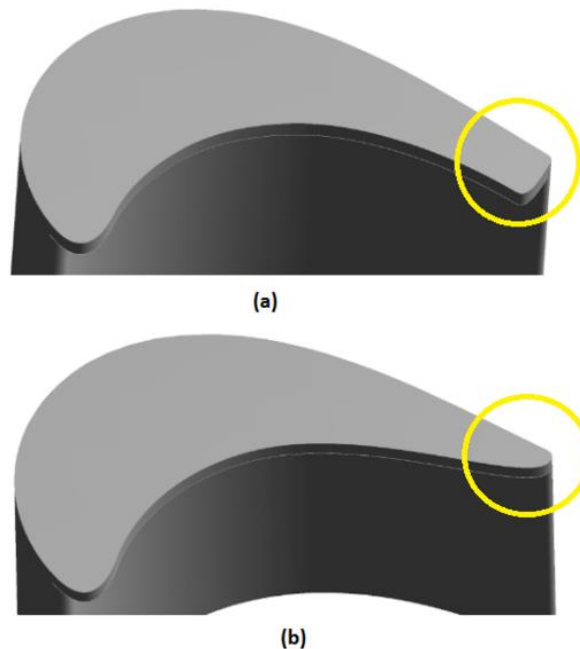
Figure 6 – Studied winglet geometries: (a) *W1*; (b) *W2*.

Unstructured meshes are used in the development of this work due to the complexity of the studied geometries. The use of these meshes implies a higher computational cost since each mesh element has a different number of neighbors, making it necessary to use connectivity tables [29]. However, these meshes are more adaptable to complex geometries [30]. Regarding the results obtained,

different works demonstrate that structured and unstructured meshes present comparable results, such as [31]. Furthermore, previous works [18] analyzing this same turbine, demonstrated that both these mesh types present comparable results.

The mesh independence study was carried out by generating four different meshes for each winglet geometry. There are no results related to the independence of the flat tip, since the results of this geometry come from previous works [18], as mentioned before.

The characteristics of these meshes are presented in Table 1.

Table 1 – Meshes characteristics.

Geometry	Number of Elements (millions of elements)		Number of Prism layer	
	W1	W2	W1	W2
Mesh 1	6.9	6.5	25	25
Mesh 2	8.4	7.8	25	25
Mesh 3	11.0	10.8	25	25
Mash 4	15.0	15.0	25	25

Note that the meshes of both geometries have a large number of elements. Part of this high amount of elements is a result of the number of prism layers used. These prism layers, however, were used to keep y+ values low. More details about this parameter, related to the turbulence model used, will be highlighted later.

The mesh independence study was performed for a 3,477 rpm rotational speed. The boundary conditions at the stage inlet and outlet were set as 1.30200 kg/s mass flow rate and 417,000 Pa static pressure respectively. Figures 7 and 8 show the results of total pressure at the rotor trailing edge region for *W1* and *W2* geometries, respectively. These figures show the results of all meshes generated.
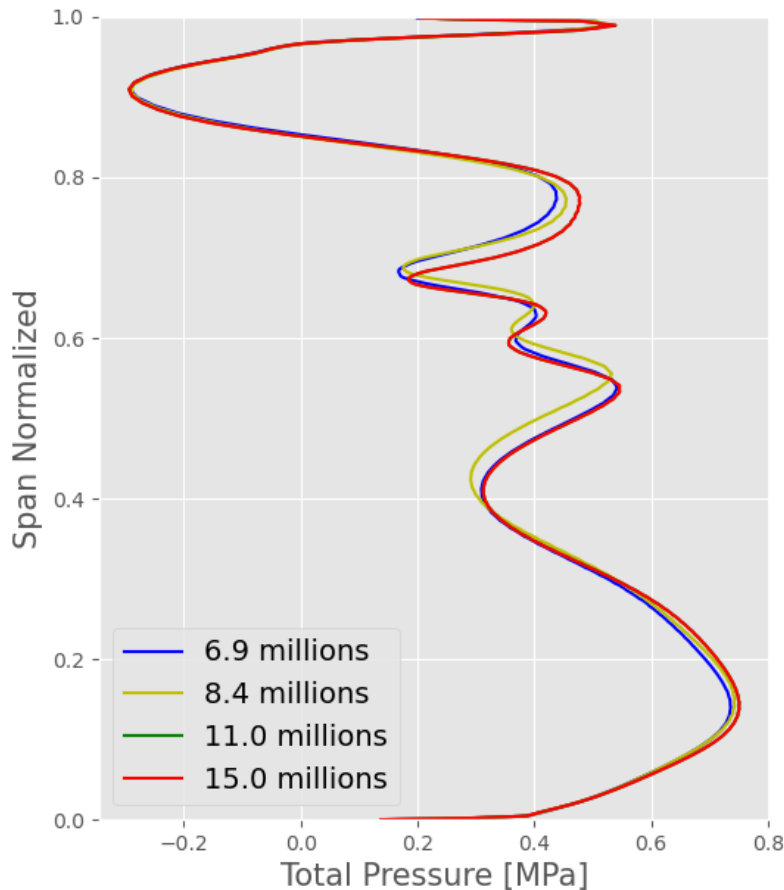
Figure 7 – Total pressure distribution at rotor trailing edge for the *W1* winglet geometry.
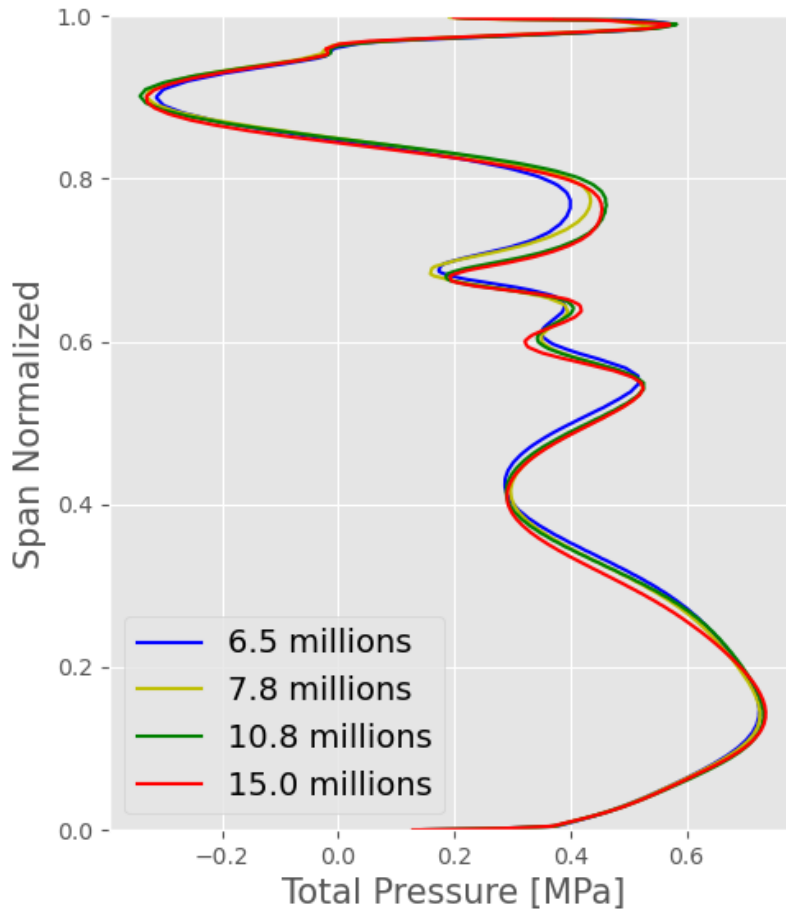
Figure 8 – Total pressure distribution at rotor trailing edge for the *W2* winglet geometry.

As can be seen from these Figures, for both geometries studied, there is little variation in the total pressure between the meshes. It is then demonstrated that the mesh refinement increase will not modify the results, and therefore it is considered that independence has already been reached. Considering the computational cost, the authors chose to use mesh 2 of both geometries to perform the calculations in this work.

Table 2 presents the y+ values obtained for each of the selected meshes.

Table 2 – Y+ at rotor blade of each mesh.

Geometry	y+ (average)
W1	0.0267 – 0.8232
W2	0.0139 – 0.8200

As can be seen, for both meshes used, the value of y+ remains below 2. This parameter is extremely important, as it will define, depending on the turbulence model used, if will be necessary to use wall functions in the calculations. Regarding the used turbulence model, Shear Stress Transport (SST), this will activate the wall functions if the parameter y+ is greater than 2. In this way, considering the chosen meshes, the wall functions will be kept off during the numerical analysis. Naturally, this also contributes to a higher computational cost, as the CFD solver will integrate the equations from the turbulence model to the wall.

5. Boundary conditions and numerical issues

The boundary conditions are the same for both meshes, and are identical to those used in [18], [21] and [32] as follows:

- At outlet: average static pressure at mid-blade height and its determination using radial equilibrium equation;

6

- At inlet: mass flow, inflow velocity vector angles (axial direction), total temperature (294 K) and turbulent intensity (5%);
- At blade-to-blade surfaces: periodicity;
- At blade rows interface: mixing-plane.
- At walls: non-slip condition.

The results obtained in this work will be compared with those of previous works [18], in addition to experimental results released by NASA [19]. In these experiments cited [19], the total pressures at the stage inlet and outlet were kept constant at 2,410,000 Pa and 550,000 Pa, respectively, for the entire turbomachine operational range. Unfortunately, the software used for the analyzes presented in this work, CFX v. 19.2, does not allow using the total pressures as a boundary condition. In this way, as was done in previous works [18], [21] and [32], the boundary conditions at the stage inlet and outlet (mass flow and static pressure, respectively), were varied until the total pressure values in these regions were at a tolerance of ±0.1% of the nominal values, informed in the experimental tests report [19]. This procedure was used to obtain the results of both studied geometries.

Table 3 presents the values of stage inlet mass flow and stage outlet static pressure for each of the evaluated Winglet geometries. As can be seen in this table, the values used for each mesh are different. This is because, for both geometries, the total pressure values at the stage inlet and outlet must agree with those indicated in the experimental results. In this table, it is also noted that, for geometry *W1*, some of these operating conditions do not present their boundary condition values. This is related to numerical instability issues that will be discussed later in this document.

Table 3 – Boundary conditions used for each winglet geometry

N [rpm]	*W1*		*W2*	
	ṁ [kg/s]	p_e [Pa]	ṁ [kg/s]	p_e [Pa]
4500	1.27770	382,350	1.28170	376,500
4159	1.28120	401,000	1.28650	391,300
3818	1.28880	415,900	1.29250	408,500
3600	1.30120	415,000	1.30670	410,500
3477	1.30700	412,200	1.31200	412,000
3136	1.32550	407,000	1.33010	409,000
2795	-	-	1.35050	395,000
2454	-	-	1.36980	361,000
2113	-	-	1.38780	330,600

CFX v. 19.2 software was used to solve the Reynolds Averaged Navier-Stokes (RANS) equations. This software is distributed by ANSYS company. The convective terms of the momentum equations were discretized using a second-order scheme, while the convective terms of the turbulence model were discretized using a first-order scheme. The two equations k-ω SST turbulence model was used to determine the flow eddy viscosity. The modified Rhie-Chow discretization method [33] was used to perform the coupling of the RANS equations. An implicit time step was used for all simulations, and its description can be found in the software manual [17].

The RMS residuals of the continuity, momentum, and energy equations are shown in Figure 9. It is possible to visualize some peaks in this figure. These represent iterations in which changes were made in the stage inlet and outlet boundary conditions so that the total pressures in these regions were close to those indicated in the available experimental results [19]. The data reported in Table 3 refer to the end of this process.

Figure 10 shows the behavior of the total pressures at the stage inlet and outlet, and the pressure ratio, along with the iterations. These properties were monitored to follow the numerical convergence, and all operating conditions presented followed this procedure.

An important point to be highlighted refers to the working fluid. According to the published report [19], the tests of the turbine studied in this work were conducted using water, despite operating with LOX. Thus, the simulations presented were also carried out considering water as working fluid.
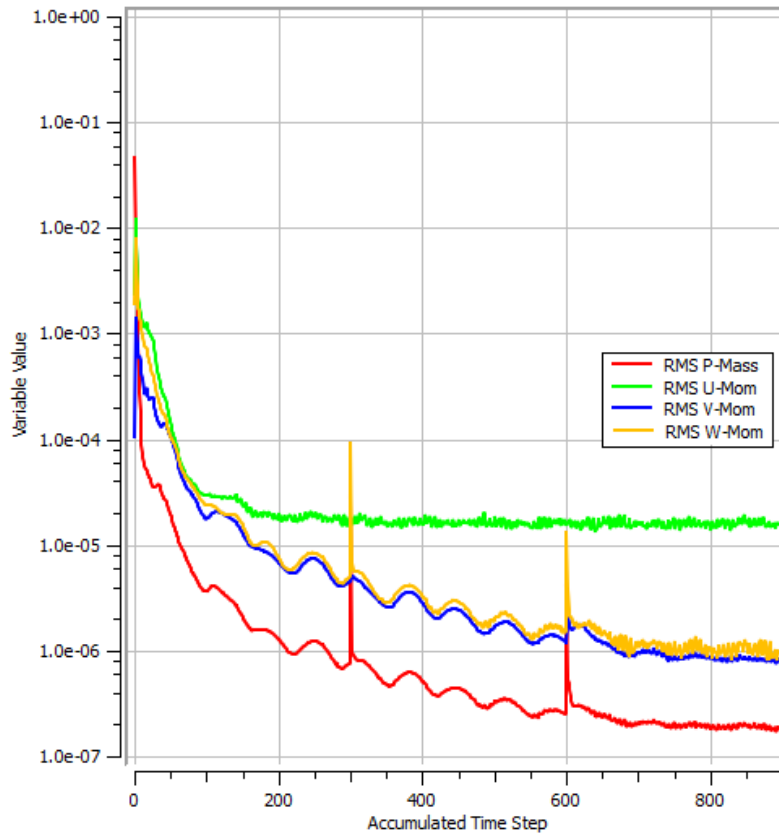
Figure 9 – Representation of the numerical residues obtained during the simulations.
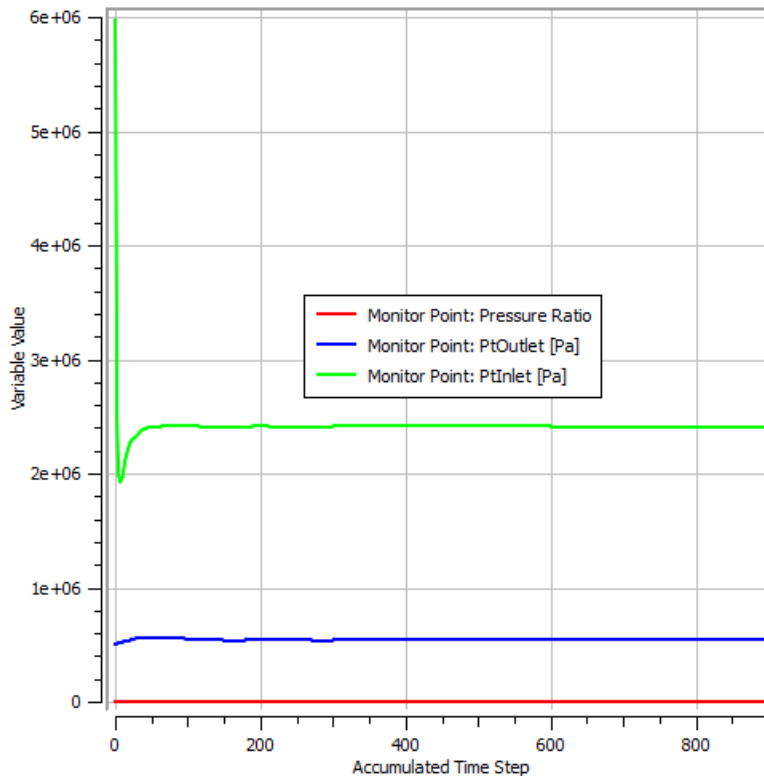
Figure 10 – Pressure ration, inlet and outlet total pressure during the simulations.

6. Comparative study between different winglet geometries

Table 4 shows the total pressure results at the stage inlet and outlet. These are the results obtained for both Winglet geometries studied in this work, using as boundary conditions the data shown in Table 3, as previously mentioned. As can be seen in these results, the tolerance of ±0.1% between

the numerical results and the experimental boundary conditions was respected for all operational conditions evaluated. Considering the flat tip, the results of this geometry can be seen in [18].

Table 4 – Results of total pressure at inlet and outlet for the *W1* and *W2* winglet geometries.

N [rpm]	W1		W2	
	$p_{T,i}$ [Pa]	$p_{T,e}$ [Pa]	$p_{T,i}$ [Pa]	$p_{T,e}$ [Pa]
4500	2,408,591	550,078	2,410580	550,058
4159	2,409,102	550,465	2,410,310	550,324
3818	2,410,516	550,039	2,408,950	550,153
3600	2,412,330	550,029	2,410,490	550,074
3477	2,408,359	549,575	2,410,110	550,051
3136	2,408,256	550,157	2,409,440	549,884
2795	-	-	2,410,800	549,735
2454	-	-	2,408,650	550,166
2113	-	-	2,409,420	549,664

As was also seen in previous works, operational conditions far from the design point (DP) presented some issues during the convergence process. Considering the *W2* geometry, for the operational conditions of 2113, 2454, and 2795 rpm, stage inlet and outlet total pressure, and pressure ratio, fluctuated around an average value (similar to what has already been found in [18]). Figure 11 shows this behavior for the rotational speed of 2795 rpm.

Regarding the *W1* geometry, also for the rotations of 2113, 2454, and 2795 rpm, numerical instability issues were also found, and the results of numerical simulations for these operating conditions diverged. For this reason, in Tables 3 and 4, the data of these operational conditions for geometry *W1* are not presented.
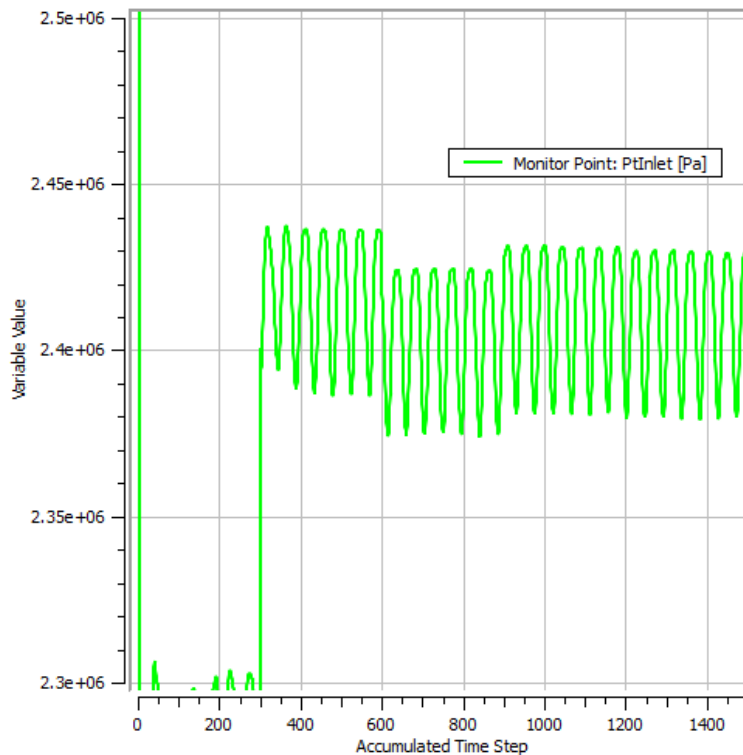
Figure 11 – Inlet total pressure at 2113 RPM, for *W2* geometry.

These behaviors found in operating conditions far from the DP are mainly related to two aspects. The first is the flow transient nature under operational conditions far from the design point. Under these conditions, instabilities inherent to the turbomachine operation will arise. The design point of the studied axial turbine is close to 3600 rpm (U/C0 ~ 0.47). For operational conditions close to this

rotational speed numerical instability issues were not found. As already mentioned in previous works [18], it is possible that for low rotational speeds, the flow unsteadiness makes the mixing-plane boundary condition invalid. It should be noted that for unsteady regimes, the mixing-plane condition is not able to determine the flow behavior between different rows. The second aspect related to instability in these operational conditions is the flow in the rotor blades trailing edge region. As will be discussed throughout this section, for geometry W1, a large wake region forms at the trailing edge region. This intensifies the flow unsteadiness, and the simulations at low rotational speeds diverge. Finally, it should be mentioned that, for the *W2* geometry, in the simulations with rotational speeds of 2113, 2454, and 2795 rpm, the average of the last 200 iterations was used as a representative value of the stage inlet and outlet total pressures.

Figure 12 shows the comparison between the efficiencies calculated through the results obtained with the numerical simulations, in addition to the results obtained for the simulations with the flat tip geometry [18], and the results of the experimental tests [19].
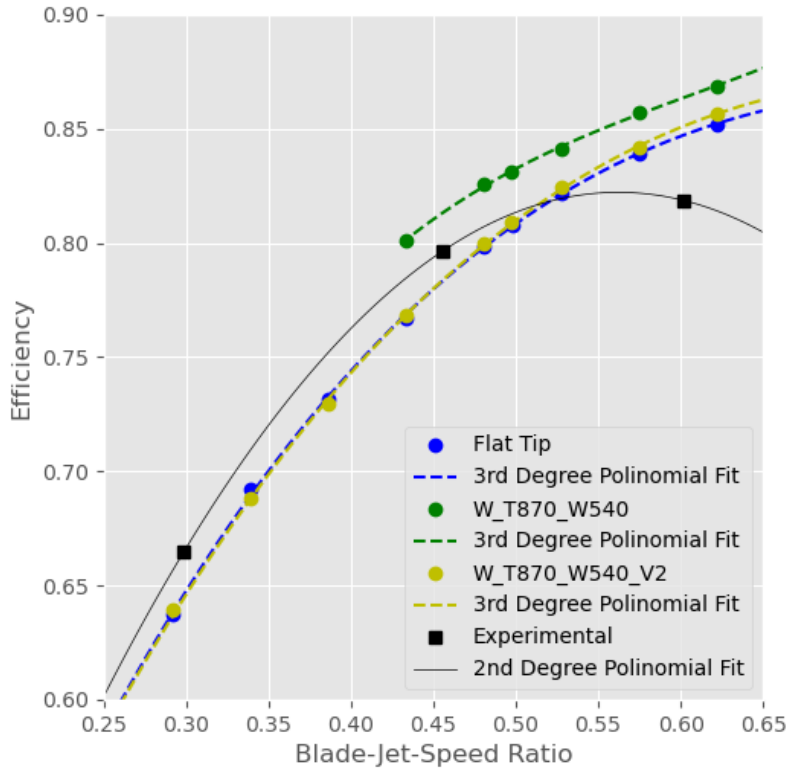
Figure 12 – Comparison between *W1*, *W2* and Flat Tip geometries results and experimental data.

The total efficiency results, as well as the blade-jet-speed ratio parameter, presented in Figure 12, were calculated through equations (1) and (2) [34], respectively.

$$\eta_{TT} = \frac{2\pi N\tau}{60 \cdot Z \cdot \left(p_{T,i} - p_{T,e}\right) \cdot \frac{\dot{m}}{\rho}} \qquad (1)$$

$$\frac{U}{C_0} = \frac{2\pi NR}{60 \cdot \sqrt{2 \cdot \left(p_{T,i} - p_{T,e}\right) \cdot \frac{1}{\rho}}} \qquad (2)$$

As shown in Figure 12, the results obtained through numerical simulations are followed by third-degree polynomial regression. Considering the experimental results, these are followed by a second-degree regression, as only three operating conditions were available in the studied operating range. This approach has already been used in previous works [18], [21] and [32], and allows a quantitative comparison to be made of the results obtained with the Winglet geometries and the flat tip geometry. The coefficients of each of the Figure 12 polynomial fit are presented in Table 5, while the quantitative

comparison between the geometries is presented in Table 6.

Table 5 – Polynomial fits coefficients.

$$\eta_{TT} = A \cdot \left(\frac{U}{C_0}\right)^3 + B \cdot \left(\frac{U}{C_0}\right)^2 + C \cdot \left(\frac{U}{C_0}\right) + D$$

	A	B	C	D
Experimental	0	-2.2662	2.5480	0.1060
Flat Tip [18]	0.9652	-2.7546	2.5353	0.1088
W1	3.2998	-6.0235	3.9295	-0.0389
W2	0.7518	-2.4231	2.3893	0.1270

Table 6 – Efficiency comparison between Flat Tip, *W1* and *W2* geometries.

Point Type	U/C_0	Percentage Differences Relative to Flat Tip [%]	
		W1	W2
DP	0.4706	2.7864	0.0676
Experimental	0.2983	-	-0.1515
	0.4559	2.9793	0.03270
	0.6017	1.6386	0.3895
	0.2922	-	-0.1478
	0.3289	-	-0.1547
	0.3656	-	-0.1291
	0.4023	-	-0.0772
	0.4390	3.1966	-0.0053
	0.4757	2.7197	0.0801
	0.5124	2.2597	0.1728
	0.5491	1.8859	0.2664
	0.5858	1.6676	0.3546
	0.6225	1.6738	0.4311

As can be seen from the results in Table 6, the *W2* geometry does not provide any benefit to the total efficiency of the analyzed turbomachinery. Regarding the *W1* geometry, there is a significant increase in the stage efficiency compared to the flat tip geometry. The average increase in stage efficiency for the *W1* geometry was 2.23%. However, it must be remembered that the simulations carried out for the *W1* geometry considered only a part of the axial turbine operational range. This reduced operating range used as a reference to determine the average increase in efficiency along the stage is the result of the instability generated by the *W1* geometry. These results demonstrate that the application of the *W2* geometry, considering the stage efficiency, is not a good strategy, as it makes the rotor blades geometry more complex, without any performance benefit. On the other hand, although the application of the *W1* geometry increases the average efficiency of the stage, it also adds instability to the flow, so that it was not possible to numerically evaluate part of the turbine operational range. These divergent results may indicate a reduction in the operating range of the stage, and therefore should be carefully evaluated. It should be mentioned, however, that different Winglet thickness and width values could modify this scenario.

Figures 13, 14 and 15 present the velocity at the trailing edge region for the flat tip, *W1* and *W2* geometries, respectively. Comparing these results, it is possible to notice that for the *W1* geometry the wake region is much larger. Observing the *W2* geometry results, and comparing these with the flat tip, it is possible to verify that this geometric modification reduces the wake region. This result is positive since the wake region reduction provides greater flow stability. Unfortunately, as observed in the results presented in Table 6, geometry *W2* did not provide any benefit in stage efficiency, despite the reduction in the wake region. However, the characteristic shown in Figure 15 motivates the development of new works using similar geometries with different thickness and width values.
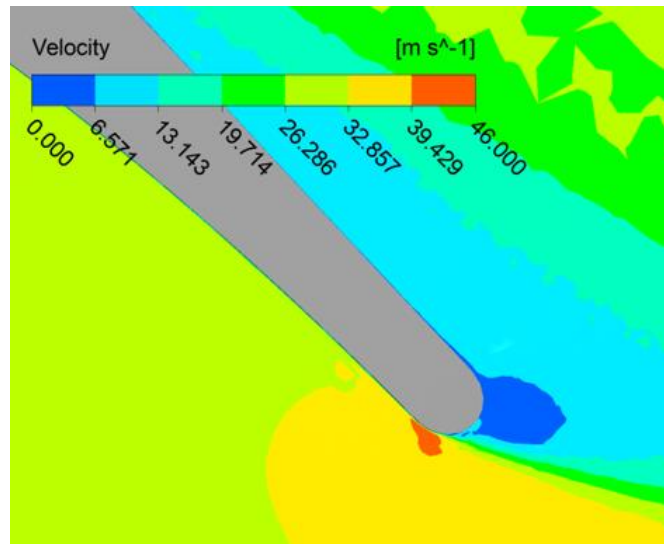
Figure 13 – Flat Tip geometry velocity field at trailing edge.
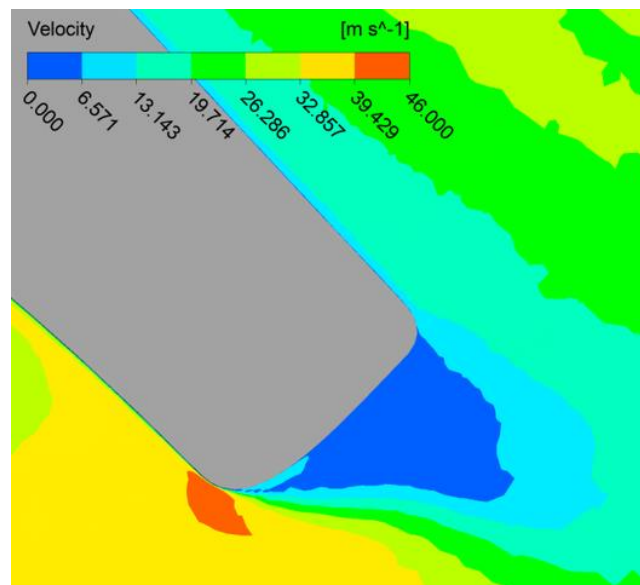
Figure 14 – *W1* winglet geometry velocity field at trailing edge.
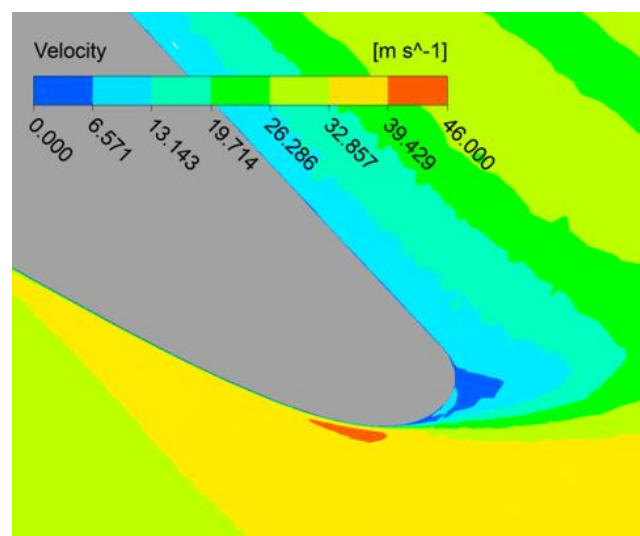
Figure 15 – *W2* winglet geometry velocity field at trailing edge.

Figures 16, 17 and 18 show entropy contours in three sections along the rotor blade, for the flat tip, *W1* and *W2* geometries, respectively. The results presented in these figures illustrate that there is a higher value of this property for the flat tip and *W2* geometries. These higher entropy values in the tip region will be related to higher irreversibilities. Naturally, as clearance has a very large influence on turbine performance, greater irreversibility in this region will also contribute to a stage efficiency reduction. This result is consistent with those shown in Table 6.
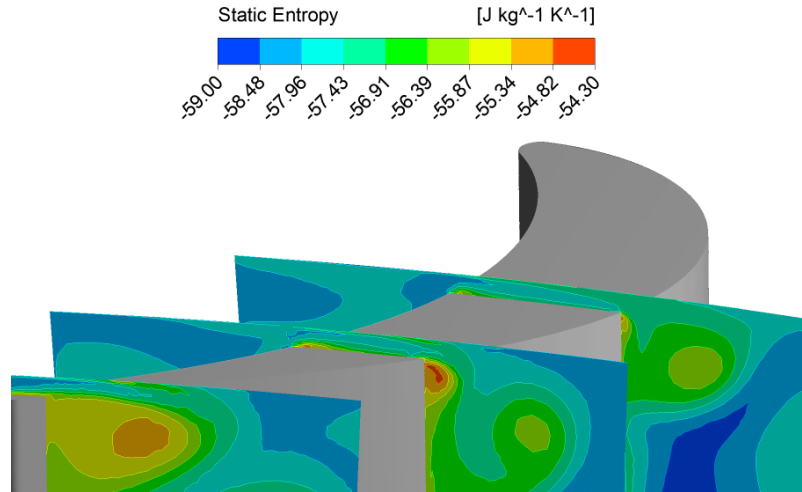
Figure 16 – Flat Tip geometry entropy contours along rotor blade.
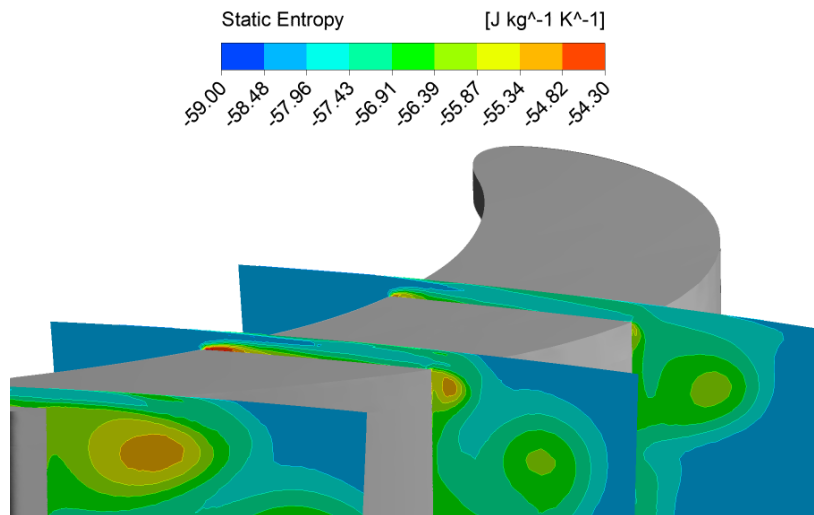
Figure 17 – *W1* winglet geometry entropy contours along rotor blade.

Finally, an evaluation of the cavitation regions throughout the stage was carried out. These regions respectively for the flat tip, W1 and W2 geometries are shown in Figures 19, 20 and 21. It is necessary to comment that all results presented in this work were obtained through monophase simulations. The cavitation is a physically two-phase phenomenon and, therefore, its evaluation is usually done through multiphase simulations. However, it has already been demonstrated in previous works that it is possible to use monophase simulations to identify the regions where this phenomenon occurs [21], [35]. Thus, the cavitation regions shown in Figures 19, 20 and 21 were obtained by generating regions in which the flow pressure reaches the water vapor pressure (2,300 Pa), thus following the same procedure as in previous works [18], [21] and [35]. Comparing Figures 19 and 20, it is noted that the application of the W1 geometry allows significant cavitation reduction at the rotor blade suction side. Regarding the W2 geometry, however, there are no changes in the cavitation regions. The results presented in Figure 20 are relevant because the cavitation reduction could increase the turbine life cycle. However, it is necessary to mention that this work analyzes only from a fluid dynamic point of view. Structural analysis to verify whether the reduction in cavitation would reflect an increase in the life cycle are necessary.
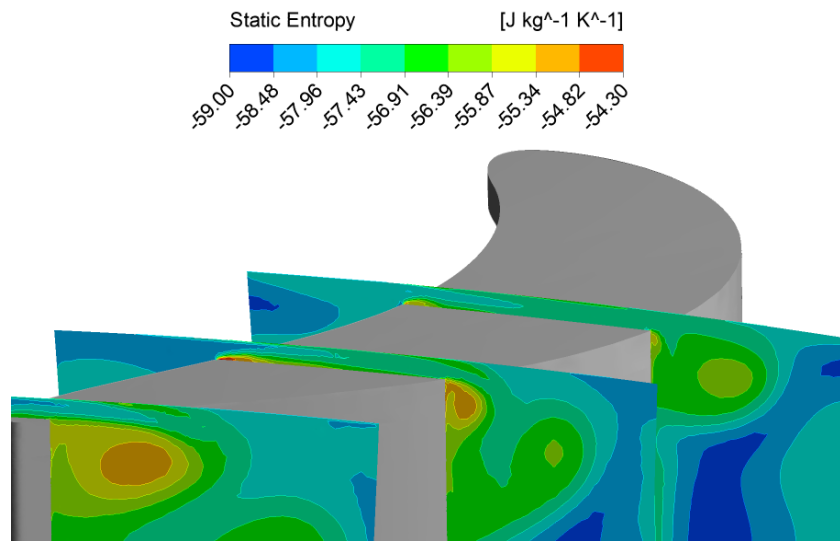
Figure 18 – *W2* winglet geometry entropy contours along rotor blade.
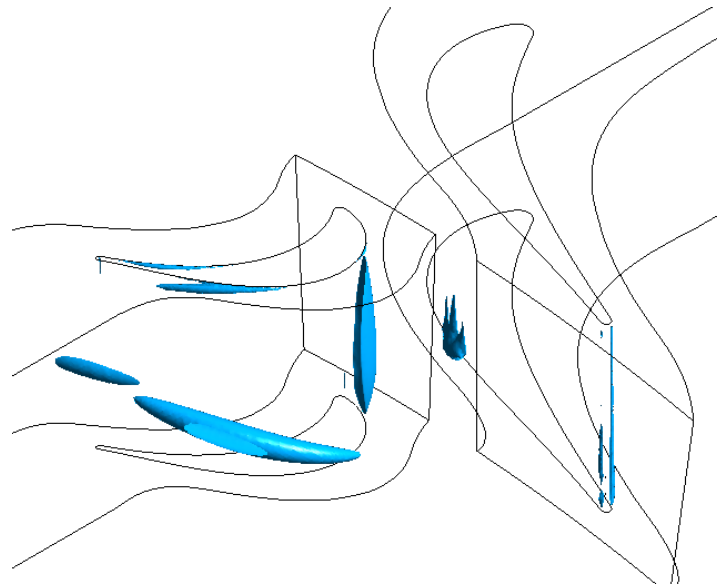
Figure 19 – Flat Tip geometry cavitation along the stage.
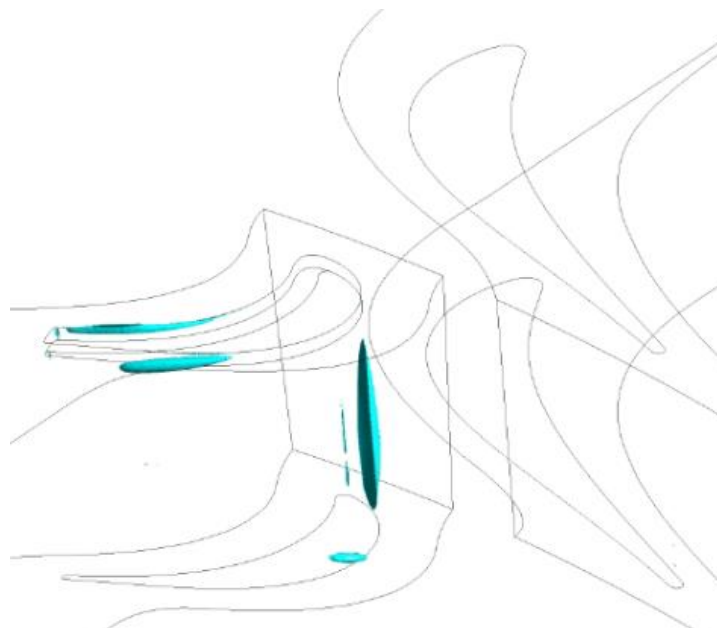
Figure 20 – *W1* winglet geometry cavitation along the stage.
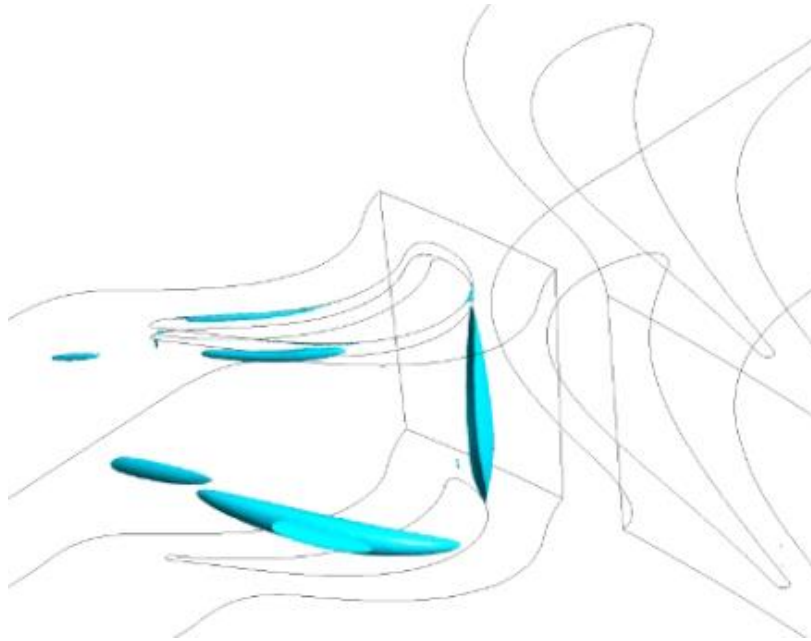
Figure 21 – *W2* winglet geometry cavitation along the stage.

Comments and conclusions

The results of this work presented a comparison between two Winglet geometries applied in the first stage of the LOX turbine used as a booster in the SSME. CFD simulations were performed using the commercial software CFX v. 19.2, distributed by ANSYS company. The original stage geometry, as well as flat tip results, were obtained from previous works [18], [21]. The boundary conditions, and the procedures used in this work, are compatible with the previous ones.

Unfortunately, during the simulation process, some difficulties related to simulation instability arose. Considering *W2* geometry, some simulations results were obtained through the average of the last 200 iterations, due to total pressure oscillations at the stage inlet and outlet. This procedure was used only for the lowest rotational speeds, which are far from the design point, and these same characteristics have already been observed in previous works [18]. Regarding the *W1* geometry, unfortunately, for these lower rotations, the simulations diverged, making it impossible to obtain the results and limiting the analyzed operating range.

Stage performance analysis with the application of each of these geometries is presented in Figure 12 and Table 6. As can be seen in these results, the application of geometry *W1* allows increasing the total efficiency of the stage by 2.23% on average. This result indicates a possible fuel consumption reduction, increasing the engine autonomy and reducing operational costs. Considering the *W2* geometry, this did not allow any performance benefit when compared to the flat tip.

Figures 13 to 15 show the wake regions in the trailing edge for each of the analyzed geometries. The results presented in these figures demonstrate that the *W2* geometry enables a reduction in this wake region. This reduction is relevant, as it would increase the flow stability. Concerning geometry *W1* (results of Figure 14), it is noticed that it generates a larger wake region. This larger wake region increases the flow instability, which may be related to the divergence of results in the simulations at low rotational speeds.

Entropy contours for each geometry are also presented (Figures 16 to 18), in which it is noted that this property has a higher value in the tip region of the flat top and *W2* geometries. This higher entropy value in this region corroborates with the stage efficiency results obtained since a higher value of this property will also be linked to greater irreversibilities. These results are even more relevant because this higher entropy value is close to the tip region, which has a very large influence on turbine performance.

Finally, Figures 19, 20 and 21 present the results regarding the cavitation regions in the flow for the flat tip, *W1* and *W2* geometries, respectively. Comparison between the *W1* and flat tip geometries illustrates that the application of this geometric modification would reduce part of this undesirable phenomenon. This reduction indicates that it would be possible to increase the stage life cycle through

the application of the *W1* geometry, however, work must be carried out evaluating the issues related to mechanical resistance. Comparing the flat tip and *W2* geometries, no significant changes in cavitation along the stage are identified.

In general, the work demonstrates the potential of desensitization techniques application in hydraulic axial turbines, and two Winglet geometries were analyzed. Regarding the *W1* geometry, this allows an increase in efficiency and a reduction in the cavitation regions in the studied stage; however, it is necessary to emphasize that problems related to flow stability arose. For the *W2* geometry, no improvements were observed in the stage efficiency or cavitation, however, there is a reduction in the wake region; this reduction indicates a flow stability increase. This greater stability motivates the development of new works, evaluating similar geometries, however, with different thickness and width dimensions, aiming to improve the parameters related to performance, maintaining the observed stability.

Acknowledgments

Copyright Statement

References

[1] Da Silva L M. *Cálculo do escoamento em uma turbine axial de alta pressão com diferentes configurações na geometria de topo do rotor utilizando técnicas de CFD.* MSc Thesis, Aeronautics Institute of Technology, São José dos Campos, São Paulo, Brazil, 2012.

[2] Zou, Z, Xuan L, Chen Y and Shao F. Effects of flow structure on heat transfer of squealer tip in a turbine rotor blade. *International Communications in Heat and Mass Transfer,* Vol. 114, No. 104588, pp 1-14, 2020.

[3] Lee S W, Jeong J S and Hong I H. Chord-wise repeated thermal load change on flat tip of a turbine blade. *International Journal of Heat and Mass Transfer,* Vol. 138, pp 1154-1165, 2019.

[4] Sakaoglu S and Kahveci H S. Effect of cavity depth on thermal performance of a cooled blade tip under rotation. *International Journal of Heat and Mass Transfer*, Vol. 143, No. 118561, 2019.

[5] Moustapha S H, Zelesky M F, Baines N C and Japikse. *Axial and Radial Turbines*. Concepts NREC, 2003.

[6] Saravanamuttoo H I, Rogers G F C and Cohen H. *Gas Turbine Theory*. 5th edition, Prentice Hall.

[7] Sjolander S A and Amrud K K. Effect of Tip Clearance on Blade Loading in a Panar Cascade of Turbine Blades. *Proc of the ASME Turbo Expo 1986*, Oregon, No. 86-GT-245, 1986.

[8] Schaug U W, Vlasic E and Moustapha S H. Effect of Tip Clearance on the Performance of a Highly Loaded Turbine Stage. *Proc of the Technology Requirements for Small Gas Turbines*, Montreal-Canada, No. 29, 1993.

[9] Booth T C, Dodge P R and Hepworth H K. Rotor-Tip Leakage: Part I - Basic Methodology. *Journal of Energy and Power*, Vol. 104, pp 154-161, 1982.

[10] Harvey N W. *Aerothermal Implications of Shroudless and Shrouded Blades*. Rhode-St-Genèse, BE: Von Karman Institute for Fluid Dynamics, 2004.

[11] Betz A. Uber die Vorgangen Den Schaufel-Endenyon Kaplan-turbinen. *Hydraulische problem*, Berlin: VDI – Verlag, 1926.

[12] Whitacker L H L. *Determinação da Influênica da folga de topo na Eficiênica de uma Turbina Axial Multiestágio utilizada em Booster de Motor Foguete para operação com LOX*. MSc Thesis, Aeronautics Institute of Technology, São José dos Campos, São Paulo, Brazil, 2017.

[13] Ainley D G and Mathieson G C R. A Method of Performance Estimation of Axial Flow Turbines. *Aero Research

Council Reports and Memoranda, No. 2974, 1951.

[14] Dunham J and Came P M. Improvements to the Ainley-Mathieson method of Turbine Performance Prediction. *Journal of Energy and Power*, Vol. 92, No. 3, pp 252-256, 1970.

[15] Kacker S C and Okapuu U. Mean Line Prediction Method for Axila Flow Turbine Efficiency. *Journal of Energy and Power*, Vol. 104, No. 1, pp 111-119, 1982.

[16] Moustapha S H, Kacker S C and Tremblay C. An Improved Incidence Losses Presiction Method for Turbine Airfoils. *Journal of Turbomachnery*, Vol. 112, pp 267-276, 1990.

[17] ANSYS CFX. *Solver theory guide*. Release 19.2. ANSYS Inc.

[18] Tonon D S, Tomita J T, Garcia E C, Bringhenti C, Díaz R B and Whitacker L H L. Comparative Study Between Structured and Unstructured Meshes Applied in Turbopump's Hydraulic Turbine. *Proc of the ASME Turbo Expo*, Online Conference, Vol. 6, No. GT2020-15004, pp 1-13, 2020.

[19] Boyton J L and Rohlik H E. Effect of Tip Clearance on Performance of Small Axial Hydraulic Turbine. *National Aeronautics and Space Administration*, Lewis Research Center, Cleveland, No. TM X-3339, 1976.

[20] UNITED STATES. *Space Transportation System Training Data - Space Shuttle Main Engine Orientation*. Boeing, 1998.

[21] Whitacker L H L, Tomita J T and Bringhenti C. An Evaluation of the Tip Clearance Effects on Turbine Efficiency for Space Propulsion Applications Considering Liquid Rocket Engine Using Turbopumps. *Aerospace Science and Technology*, Vol. 70, pp 55-65, 2017.

[22] Dey D and Camci C. Aerodynamic tip desensitization of an axial turbine rotor using tip platform extensions. *Proc of the ASME Turbo Expo*, New Orleans, No. GT-0484, pp 1-17, 2001.

[23] Lee S W, Kim S U and Kim K H. Aerodynamic performance of winglets covering the tip gap inlet in a turbine cascade. *International Journal of Heat and Fluid Flow*, Vol. 34, pp 36-46, 2012.

[24] Zhou C, Hodson H, Tibbott I and Stokes M. Effects of winglet geometry on the aerodynamic performance of tip leakage flow in a turbine cascade. *Journal of Turbomachinery*, Vol. 135, pp 1-10, 2013.

[25] Cheon J H and Lee S W. Winglet geometry effects on tip leakage loss over the plane tip in a turbine cascade. *Journal of Mechanical Science and Technology*, Vol. 32, No. 4, pp 1633-1642, 2018.

[26] Seo Y C and Lee S W. Tip gap flow and aerodynamic loss generation in a turbine cascade equipped with suction-side winglets. *Journal of Mechanical Science and Technology*, Vol. 27, No. 3, pp 703-712, 2013.

[27] Coull J D, Atkins N R and Hodson H P. Winglets for improved aerothermal performance of high pressure turbines. *Journal of Turbomachinery*, Vol. 136, pp 1-11, 2014.

[28] Lee S W, Cheon J H and Zhang Q. The effect of full coverage winglets on tip leakage aerodynamics over the plane tip in a turbine cascade. *International Journal of Heat and Fluid Flow*, Vol. 45, No. 1, pp 23-32, 2014.

[29] Tomita J T, da Silva L M and da Silva D T. Comparison between unstructured and structured meshes with different turbulence models for a high pressure turbine application. *Proc of the ASME Turbo Expo*, Copenhagen, Vol. 8, No. GT2012-69990, pp 1633-1645, 2012.

[30] Blazek J. *Computational Fluid Dynamics: Principles and Applications*. 3th edition, Elsevier, 2015.

[31] Contreras J, Corral R, Fernandez-Castañeda J, Pastor G and Vasco C. Semi-Unstructured Grid Methods for Turbomachinery Applications. *Proc of the ASME Turbo Expo*, Amsterdan, No. GT2002-30572, 2002.

[32] Barbosa D F C, Tonon D S, Whitacker L H L, Tomita J T and Bringhenti C. Evaluation of Different Turbulence Models Applied in Turbopump's Hydraulic Turbine. *Proc of the ASME Turbo Expo*, Online Conference, Vol. 2C, No. GT2021-59414, pp 1-15, 2021.

[33] Rhie C M and Chow W L. A Numerical Study of the Turbulent Flow Past an Isolated Airfoil with the Trailing Edge Separation. *AIAA*, No. 82-0998, 1982.

[34] Whitacker L H L, Tomita J T and Bringhenti C. Turbopump Booster Turbine Performance: Comparison between Monophase and Multiphase Flows Using CFD. *Proc. of the ASME Turbo Expo*, Oslo, Vol. 2B, No. GT2018-76879, pp 1-9, 2018.

[35] Whitacker L H L, Tomita J T and Bringhenti C. Effect of Tip Clearance on Cavitating Flow of a Hydraulic Axial Turbine Applied in Turbopump. *International Journal of Mechanical Sciences*, Vol. 213, pp 106855, 2022.